

Diphoton Signals from Colorless Hidden Quarkonia

Sho Iwamoto,^{*} Gabriel Lee,[†] and Yael Shadmi[‡]
*Physics Department, Technion—Israel Institute of Technology,
Haifa 32000, Israel*

Robert Ziegler[§]
*Sorbonne Universités, UPMC Univ Paris 06, UMR 7589, LPTHE, F-75005, Paris, France
CNRS, UMR 7589, LPTHE, F-75005, Paris, France*
(Dated: November 9, 2018)

We show that quarkonia-like states of a hidden $SU(N)$ gauge group can account for the 750 GeV diphoton excess observed by ATLAS and CMS, even with constituents carrying standard model hypercharge only. The required hypercharge is modest, varying between about 1.3–1.6 for strong $SU(N)$ coupling, to 2–3 for weak $SU(N)$ coupling, for $N = 3, 4$. This scenario predicts a variety of diphoton and multi-photon resonances, as well as photons from continuum pair production, and possibly exotic decays into standard model fermions, with no significant multi-jet resonances.

INTRODUCTION

If new particles are produced at the LHC, they have so far eluded detection, suggesting some suppression of their decays. In the presence of such suppression, bound states of these particles can be produced near threshold. Diphoton resonances from bound-state decay may then be the first harbingers of new physics. In this paper, we interpret the excess of diphoton events near 750 GeV reported by the ATLAS [1–3] and CMS [4–6] Collaborations as arising from the decay of a “quarkonium”-like state, η_X , bound by a hidden confining $SU(N)$. Our model is minimal in that it assumes photoproduction as the main η_X production channel [7–9]. Thus, we take the η_X constituents X to carry hypercharge only, but no standard model (SM) $SU(3)_c$ or $SU(2)_L$ quantum numbers. This is in contrast to similar recent work which featured bound states with colored constituents [10–19]. While the production cross section is controlled by the hypercharge of the constituents, Y_X , and is proportional to Y_X^4 , bound-state formation is controlled by the new strong force.

We will focus on the possibility that the constituents X are vector-like fermions in the (anti-)fundamental representation of the hidden $SU(N)$.¹ The lowest-lying $J = 0$ bound state is mainly produced via vector-boson fusion (VBF) processes, especially $\gamma\gamma$ fusion, while Drell–Yan (DY) production gives $J = 1$ bound states.

Below we discuss two limiting cases, for which the bound-state properties can be readily estimated. In the first, the $SU(N)$ is weakly coupled, such that the $SU(N)$ confinement scale Λ_h is much smaller than the constituent mass m_X . The bound state is governed by the Coulomb $SU(N)$ potential in this case, so that its

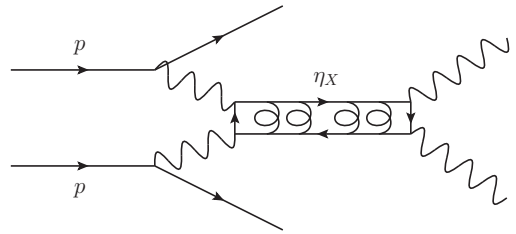


FIG. 1. Photoproduction of the bound state η_X at the LHC. Gluon lines are for the hidden sector $SU(N)$.

properties and production cross section can be calculated perturbatively. In the second, the $SU(N)$ is strongly coupled, and confinement effects are important. We will then rely on analogies with measured QCD quantities, mainly in the charmonium system, to infer the properties of η_X . For simplicity, we restrict our attention to high values of Λ_h , such that η_X decays into hidden glueballs are kinematically forbidden. We stress that intermediate values of Λ_h can easily account for the diphoton signal, but we cannot give any quantitative estimate of branching ratios, binding energies etc. in this region.

In either case, with no light $SU(N)$ flavors, the models obtained are quirk-like models [12, 13, 20–22] with uncolored quirks and relatively large Λ_h , which leads to microscopic strings. The distinguishing signatures of the models are a variety of multi-photon signatures, with di-jet or multi-jet resonances absent or suppressed. In addition to diphoton events from bound-state decays, $X\text{--}\bar{X}$ pair production above threshold also gives multi-photon final states, either directly from annihilations into photons, or from annihilations into hidden glueballs which in turn decay into photons (or SM fermions).

We also consider models with additional light $SU(N)$ flavors, which are SM-singlets, with couplings to X and SM fields. $X\text{--}\bar{X}$ pair production above threshold then gives a pair of X -hadrons which decay to SM fields through those couplings.

¹ Scenarios with scalar constituents are possible as well, leading to different phenomenology. For example, the DY production of $J = 1$ state is suppressed due to the lack of spin.

TABLE I. Summary of the hidden $SU(N)$ and the SM charges of the new vector-like fermion X .

	$SU(N)$	$SU(3)_c, SU(2)_L, U(1)_Y$
X	N	$(1, 1, Y_X)$
\bar{X}	\bar{N}	$(1, 1, -Y_X)$

This paper is organized as follows. We begin by reviewing the required cross section to diphotons and decay rates for the bound states. We describe two scenarios, roughly corresponding to small and large hidden couplings, in which diphoton decays of the lightest $X\bar{X}$ bound state in the hidden sector can yield the correct signal. We discuss the phenomenology of the hidden sector, including the possibility of excited bound states and LHC signals from pair production of $X\bar{X}$. Possible decays of X itself are considered before we conclude.

THE η_X BOUND STATE AND DIPHOTON SIGNAL STRENGTH

We begin with an overview of the different scales in the hidden sector. For concreteness, we assume that the 750 GeV resonance is a 1^1S_0 bound state η_X of a fundamental Dirac fermion X of mass m_X and hypercharge Y_X (cf. Table I).² The required cross section is [16]

$$\sigma(pp \rightarrow \eta_X \rightarrow \gamma\gamma) \Big|_{\sqrt{s}=13 \text{ TeV}} \sim 3\text{--}6 \text{ fb}. \quad (1)$$

Since its constituents are not colored, the dominant production channel for η_X is VBF, specifically photon fusion. Taking the result from Ref. [9], which includes the contributions from inelastic–inelastic, elastic–inelastic, and elastic–elastic processes, the total photoproduction signal strength at 13 TeV in the narrow width approximation is given by³

$$\sigma_{13}^{pp \rightarrow \eta_X \rightarrow \gamma\gamma} = 5 \text{ fb} \left(\frac{\Gamma_{\text{tot}}}{21 \text{ MeV}} \right) \text{Br}(\eta_X \rightarrow \gamma\gamma)^2, \quad (2)$$

where Γ_{tot} is the total decay width of η_X . $Z\gamma$ and ZZ production channels contribute an additional 8% to the cross section [23].

² Quarkonia are often labelled in the form $n_r^{2S+1}L_J$ in analogy with spectroscopic notation, where S , L , and J are the spin, orbital, and total angular momentum quantum numbers. The radial excitation number n_r is related to the principal quantum number n by $n = n_r + L$. The radial excitation number and orbital angular momentum are used in parentheses for particle-like names of quarkonia states, e.g., $J/\psi(1S)$.

³ The cross-section at 8 TeV is about a factor of 2 smaller, and thus in tension with Run 1 diphoton searches. However, this ratio is subject to potentially large uncertainties [7, 8].

Bound-state production is enhanced for $L = 0$ states by the wavefunction at the origin. The partial width of the lightest bound state η_X into photons is (cf. Ref. [18])

$$\frac{\Gamma(\eta_X \rightarrow \gamma\gamma)}{M} = 4N(Y_X^2\alpha)^2 \frac{|R_{n0}(0)|^2}{M^3}, \quad (3)$$

where $R_{n0}(r)$ is the radial wavefunction of a bound state with orbital angular momentum $L = 0$ and principal quantum number n , normalized such that $\int_0^\infty |R_{n0}(r)|^2 r^2 dr = 1$. Perturbatively, the ratio of η_X decay rates to two photons vs. two hidden gluons is

$$\frac{\Gamma(\eta_X \rightarrow \gamma\gamma)}{\Gamma(\eta_X \rightarrow g_h g_h)} = 4 \frac{N^2}{N^2 - 1} \frac{(Y_X^2\alpha)^2}{\alpha_h^2}, \quad (4)$$

where g_h denotes a hidden gluon. Below, two scenarios are considered: one with small α_h such that the decay rates to diphotons and invisible hadrons are comparable, and one with large α_h , with the hidden glueball channel kinematically closed. We refer to these scenarios as “Low Λ_h ” and “High Λ_h ”.

Low Λ_h

For small α_h , the $SU(N)$ binding potential can be described in the Coulomb approximation [24]

$$|R_{n0}(0)|^2 = \frac{C^3 \bar{\alpha}_h^3 m_X^3}{2n^3}, \quad (5)$$

where

$$C = \frac{1}{2}(C_1 + C_2 - C_\eta), \quad (6)$$

and C_η, C_1, C_2 are the quadratic Casimirs of the bound state and its constituent particles. For constituents in the (anti-)fundamental representation and the singlet bound state of $\bar{X}X$, $C_\eta = 0$ and $C_1 = C_2 = \frac{N^2-1}{2N}$. Then

$$|R_{n0}(0)|^2 \sim \left(\frac{N^2 - 1}{2N} \right)^3 \frac{\bar{\alpha}_h^3 M^3}{16n^3}, \quad (7)$$

where we assumed that the bound-state energy $M \sim 2m_X$, and defined $\bar{\alpha}_h$ as the hidden sector gauge coupling in the $\overline{\text{MS}}$ scheme, evaluated at the Bohr radius of the bound state

$$r_{\text{rms}} \sim a_0 = 2/(C\bar{\alpha}_h m_X), \quad \bar{\alpha}_h \equiv \alpha_h(a_0^{-1}). \quad (8)$$

The decay rate into photons is then given by

$$\frac{\Gamma(\eta_X \rightarrow \gamma\gamma)}{M} = \frac{1}{4} N Y_X^4 \alpha^2 \left(\frac{N^2 - 1}{2N} \right)^3 \bar{\alpha}_h^3, \quad (9)$$

where $\alpha = \alpha(M) \approx \alpha(M_Z) \approx 1/128$.

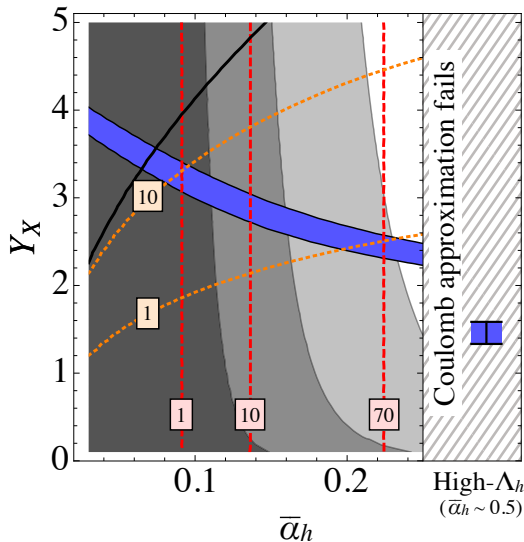


FIG. 2. Parameter space for $N = 3$. The blue band indicates the diphoton signal strength of 3–6 fb, vertical red (dashed) lines denote the lightest glueball mass M_{G_h} in GeV, and orange (dotted) lines denote the ratio $\Gamma(\eta_X \rightarrow \gamma\gamma)/\Gamma(\eta_X \rightarrow g_h g_h)$. The grey-filled regions indicate the lifetime of the lightest glueball, ranging from left to right as $\tau_{G_h} > 1$ s (dark grey), $1 \text{ s} > \tau_{G_h} > 10^{-7}$ s, $10^{-7} \text{ s} > \tau_{G_h} > 10^{-12}$ s, and $\tau_{G_h} < 10^{-12}$ s (white). The black line indicates values of $\bar{\alpha}_h$ and Y_X for which the binding energies from hypercharge and the hidden $SU(N)$ are equal. The value $\bar{\alpha}_h = 0.25$ corresponds to $\alpha_h(M) = 0.11$. At larger $\bar{\alpha}_h$, we infer the signal strength from the QCD charmonium system and show it as a preferred range of Y_X . See text for details.

The binding energy is given by (at leading order)

$$E_b = -\frac{1}{4n^2} C^2 \bar{\alpha}_h^2 m_X, \quad (10)$$

so that the mass of this bound state is ($E_b \equiv E_1$)

$$M = 2m_X + E_b = \left(2 - \frac{1}{4} \left(\frac{N^2 - 1}{2N}\right)^2 \bar{\alpha}_h^2\right) m_X. \quad (11)$$

To calculate the signal strength, we also need the partial decay rates into the hidden sector, and into different SM particles. Since the resonance couples only to hypercharge, the decay rates into $Z\gamma$ and ZZ are given by

$$\frac{\Gamma(\eta_X \rightarrow \{Z\gamma, ZZ\})}{\Gamma(\eta_X \rightarrow \gamma\gamma)} = \{2 \tan^2 \theta_W, \tan^4 \theta_W\} \approx \{0.6, 0.08\}, \quad (12)$$

where θ_W is the Weinberg angle with $\sin^2 \theta_W \approx 0.23$. Including these channels reduces the branching ratio to diphotons by about 40%.

Decays into hidden sector hadrons are dominated by annihilations into two hidden gluons, Eq. (4). With no light hidden flavors, these hadronize into hidden glueballs. For pure QCD, the lightest glueball has $J^{PC} =$

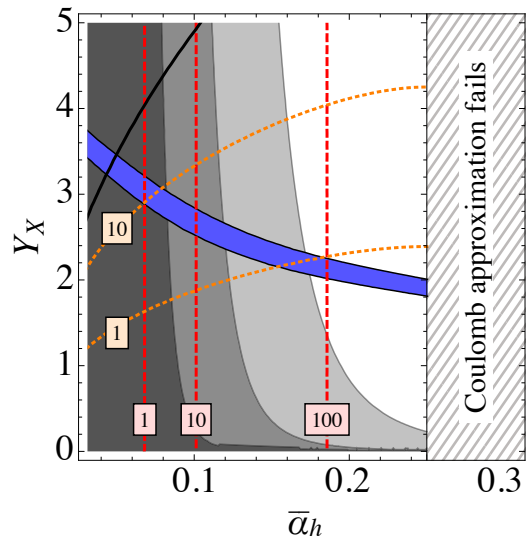


FIG. 3. Same as Fig. 2 for $N = 4$. The value $\bar{\alpha}_h = 0.25$ corresponds to $\alpha_h(M) = 0.10$.

0^{++} and mass $\sim 7\Lambda_{\text{QCD}}$ [25]. We assume the same scaling for the lightest glueball G_h of the hidden $SU(N)$, $M_{G_h} \sim 7\Lambda_h$, where the confinement scale Λ_h is given at one-loop order by

$$\Lambda_h \sim m_X \exp\left(\frac{-2\pi}{b_0 \alpha_h(m_X)}\right), \quad (13)$$

with $b_0 = \frac{11}{3}N - \frac{2}{3}N_F$, where N_F is the number of light fermion flavors. G_h mainly decays to photons through loops of X , with lifetimes estimated for $N = 3$ (see, e.g., Refs. [26–28]),

$$\Gamma(0_h^{++} \rightarrow \gamma\gamma) \approx \frac{Y_X^4 \alpha^2 M_{G_h}^3}{64\pi^3 m_X^2} \left(\frac{3M_{G_h}^3}{60m_X^3}\right)^2. \quad (14)$$

For fixed N , we are therefore left with Y_X and $\bar{\alpha}_h$ as free parameters. In Figs. 2 and 3, we show the required diphoton signal strength in the Coulomb regime as a blue band in the $\bar{\alpha}_h$ – Y_X plane for $N = 3$ and $N = 4$, respectively, with $N_F = 0$. The plots are truncated at $\bar{\alpha}_h = 0.25$, where the Coulomb approximation can no longer be trusted (see discussion below). Also indicated on the $N = 3$ plot is the range of Y_X preferred for the diphoton signal strength in the “High- Λ_h ” scenario, which is discussed in the next subsection. As expected, lower values of Y_X are preferred in this case compared to the Coulomb regime, since the enhancement factor $|R(0)|^2$ grows with the hidden coupling. In between the two regions, phenomenological potentials, which interpolate between the Coulomb and confining regimes, can be used to describe the bound states (see, e.g., Ref. [29]). Clearly, there are large uncertainties in these calculations. Thus, for example, for stoponium, a recent lattice calculation finds that potential models [30] underestimate $|R(0)|^2$ by a factor of about 4 [31]. In any case,

the effect of these modifications would be to increase the production cross section of η_X , so that the blue region would shift to smaller values of Y_X above a given α_h .

The vertical red (dashed) lines denote the lightest glueball mass in GeV; here, we determine Λ_h by solving the two-loop renormalization group (RG) equations for the boundary condition $\alpha_h(\Lambda_h) = 4\pi$. The orange (dotted) lines give the ratio $\Gamma(\eta_X \rightarrow \gamma\gamma)/\Gamma(\eta_X \rightarrow g_h g_h)$ from Eq. (4). The grey-filled regions in Figs. 2 and 3 indicate the lifetime of the lightest glueball according to Eq. (14), ranging from > 1 s in the dark grey region to prompt decays in the white region. The dark grey region is excluded by Big Bang nucleosynthesis (BBN) since energetic photons from glueball decays would dissociate nuclei. The binding energy is less than $\mathcal{O}(10 \text{ GeV})$ in this range; we have included the contribution of the hypercharge Coulomb potential to the binding energy.⁴ The solid black lines in the figures indicate values of $Y_X, \bar{\alpha}_h$ for which the contributions to the binding energy from hypercharge and the hidden $SU(N)$ are equal. For Y_X between 2–2.5, we obtain the diphoton signal for $\bar{\alpha}_h \gtrsim 0.22$ (0.18) for $N = 3$ (4), which corresponds to $\alpha_h(M) \gtrsim 0.1$ (0.08).

For very small values of α_h , the cross section becomes independent of $\bar{\alpha}_h$ and the hypercharge Coulomb potential is dominant in creating the bound state. The ratio of enhancement factors and binding energies are,

$$\frac{|R(0)|_{\text{em}}^2}{|R(0)|_h^2} \sim \left(\frac{E_{b,\text{em}}}{E_{b,h}} \right)^{3/2} \sim \left(\frac{2Y_X^2 \alpha}{N\alpha_h} \right)^3. \quad (15)$$

Above the black lines in Figs. 2 and 3, the hypercharge Coulomb interaction is dominant. In particular, we can use our results to estimate whether a purely hypercharged X can account for the signal. This requires $Y_X \sim 4$, in contrast with larger values found in Ref. [32] (taking into account the different multiplicity N in our model). Finally, we note that for $Y_X = 4$ and $N = 3$ ($N = 4$), the hypercharge coupling g_Y becomes non-perturbative at around 2000 (300) TeV due to additional running from X .

For large $\bar{\alpha}_h$, we can understand the flattening of the blue signal region in Figs. 2 and 3 from Eq. (16) as follows. It is instructive to consider how the total rate into photons scales with the $SU(N)$ parameters and Y_X . From Eqs. (2), (3), and (5), and neglecting phase space factors due to the hidden glueball mass, we have

$$\sigma(pp \rightarrow \eta_X \rightarrow \gamma\gamma) \propto Y_X^8 \left(\frac{\bar{\alpha}_h}{\alpha_h(M)} \right)^2 \bar{\alpha}_h, \quad (16)$$

which grows very fast with Y_X , and approximately linearly with the hidden coupling. In Eq. (8), we see that a_0^{-1} grows linearly with $\bar{\alpha}_h$; therefore, for large $\bar{\alpha}_h$, the hierarchy between a_0^{-1} and M itself is small, so $\bar{\alpha}_h/\alpha_h(M)$ is approximately constant. Hence, to maintain a fixed cross section, Y_X needs to change only by a small amount to compensate for a given change in $\bar{\alpha}_h$.

As α_h increases, confinement effects become important, and the Coulomb approximation becomes inadequate. Roughly speaking, this approximation is valid when the Bohr radius of the bound state is larger than the confinement scale,⁵

$$\Lambda_h \ll a_0^{-1} = \frac{C}{2} \bar{\alpha}_h m_X = \left(\frac{N^2 - 1}{4N} \right) \bar{\alpha}_h m_X. \quad (17)$$

Furthermore, the radial wavefunction at the origin $|R(0)|^2$ and the binding energy as given in Eqs. (5) and (10) are the leading-order results. Higher-order corrections to the binding energy were calculated in [33]. To obtain another estimate of the validity of the perturbative expansion, we take their result for the next-to-leading order (NLO) correction for zero light flavors,

$$E_b = E_1 \left[1 + \frac{\bar{\alpha}_h}{\pi} N \times 2.85 + \mathcal{O}(\bar{\alpha}_h/\pi)^2 \right], \quad (18)$$

which implies that we need $\bar{\alpha}_h \lesssim 0.25$ in order to trust the perturbative expansion. We therefore truncate the plots at $\bar{\alpha}_h = 0.25$. For both Figs. 2 and 3, Eq. (17) is satisfied in this region.

The above discussion assumed no light $SU(N)$ flavors for concreteness, but it can be simply extended to $N_F > 0$ light flavors with mass of order Λ_h . In this case, η_X can decay to hidden hadrons as well, whose mass is probably of order Λ_h , and lighter than the glueballs. Furthermore, Λ_h is smaller for a given α_h because of the slower running. For a single flavor, this is a mild effect, and the results of Figs. 2 and 3 will remain unchanged. In fact, the region in which the Coulomb approximation is valid will be wider in this case, allowing for larger α_h .

High Λ_h

We now turn to consider larger $SU(N)$ couplings, for which the Coulomb approximation fails. In this scenario, $|R(0)|^2$ (and hence the enhancement of bound-state production) and the binding energy are sensitive to confinement effects, and are therefore large. In addition to the diphoton rates, η_X will have large decay rates into hidden hadrons. Whether or not these are consistent with

⁴ Including the hypercharge contribution in the binding energy and the wavefunction at the origin involves the substitution $(C\bar{\alpha}_h)^n \rightarrow (C\bar{\alpha}_h + Y_X^2 \alpha)^n$ in Eqs. (5) and (10).

⁵ The potential approximation is valid for $\eta_b(1S)$, the lowest state of bottomonium, which has a separation scale $a_0 \sim 0.2$ fm compared to $\Lambda_{\text{QCD}}^{-1} \sim 1$ fm [29].

$SU(3)_c$	$SU(N)$
M_{η_c} <u>3 GeV</u>	M_{G_h} <u>0.6 – 1 TeV</u>
M_D <u>1.85 GeV</u>	M <u>750 GeV</u>
M_{G_h} <u>1.7 GeV</u>	m_X <u>400 – 450 GeV</u>
m_c <u>1.3 GeV</u>	
Λ_{QCD} <u>250 MeV</u>	Λ_h <u>90 – 150 GeV</u>

FIG. 4. Summary of scales for charmonium and QCD (left column) and for $\bar{X}X$ and the hidden $SU(N)$ (right column). Values of Λ_{QCD} in the $\overline{\text{MS}}$ scheme with various N_F can be found in Ref. [34]; the FLAG review of Ref. [35] quotes $\Lambda_{\text{QCD}} \sim 250$ MeV. The values for the scales in the right column are representative, as detailed in the text, for an example with $N = 3$.

LHC constraints is hard to estimate; so for simplicity, we focus here on very high Λ_h , such that decays to glueballs are kinematically forbidden. In fact, a particularly dangerous channel is η_X decay to a photon and an excited hidden glueball. Using again the pure QCD results of Ref. [25], the lightest allowed glueball for this decay is the 1_h^{+-} glueball, with mass $\sim 1.7M_{G_h}$. Requiring this mass to be heavier than η_X , we have

$$\Lambda_h \gtrsim 65 \text{ GeV}. \quad (19)$$

Thus, in this scenario, $\text{Br}(\eta_X \rightarrow \gamma\gamma) \sim 0.6$.⁶

Since the Coulomb approximation cannot be used to compute bound-state quantities, we must instead rely on analogies with measured QCD bound states, e.g., in the charmonium system (for a comprehensive review of quarkonia, see Ref. [29]).

TABLE II. Summary of masses and widths for lowest states of charmonium and bottomonium, from Ref. [34].

\mathcal{B}	$M_{\mathcal{B}}$ [GeV]	$(\Gamma/M)_{\mathcal{B}}$
$\eta_c(1S)$	2.984	1.1×10^{-2}
$J/\psi(1S)$	3.097	3.0×10^{-5}
$\eta_b(1S)$	9.398	1.2×10^{-3}
$\Upsilon(1S)$	9.460	5.7×10^{-6}

⁶ Note that we cannot add light $SU(N)$ flavors in this case, since the resulting mesons would provide new, dangerous decay channels for η_X .

In the charmonium case, the mass of the 1^1S_0 bound state $\eta_c(1S)$ is $M_{\eta_c} \sim 3$ GeV. The major difference in QCD is the existence of $N_F = 3$ light quarks below Λ_{QCD} . In this case, the D mesons are the effective constituents of charmonium with $M_D \sim 1.85$ GeV for the lightest D meson; therefore, the binding energy is approximately 0.6–0.7 GeV, or about 20% of the mass of $\eta_c(1S)$. We then expect $m_X \sim 400$ –450 GeV.

To obtain the decay width $\Gamma(\eta_X \rightarrow \gamma\gamma)$, we can perform a similar scaling with charmonium. Using Γ_{tot}/M for $\eta_c(1S)$ listed in Table II and $\text{Br}(\eta_c \rightarrow \gamma\gamma) = (1.59 \pm 0.12) \times 10^{-4}$, both taken from Ref. [34], we obtain

$$\begin{aligned} \frac{\Gamma(\eta_X \rightarrow \gamma\gamma)}{M} &= \frac{\Gamma(\eta_c \rightarrow \gamma\gamma)}{M_{\eta_c}} \left(\frac{Y_X}{Q_c} \right)^4 \\ &= 1.75 \times 10^{-6} \left(\frac{Y_X}{Q_c} \right)^4, \end{aligned} \quad (20)$$

where $Q_c = 2/3$ is the electromagnetic charge of the charm quark. Substituting the above for Γ_{tot} and with $\text{Br} \sim 0.6$ in Eq. (2), we thus see that the diphoton excess can be accounted for $1.3 \lesssim Y_X \lesssim 1.6$, and for a wide range of α_h (and equivalently, of Λ_h). This range is shown in the hashed region on the right-hand side of Fig. 2. Some representative values of these scales are sketched in Fig. 4; with the X mass between 400–450 GeV, Λ_h is between 100–150 GeV, and the glueballs between 600 GeV and 1 TeV, reflecting the large uncertainties in the glueball mass.

The large binding energy in this case allows for the possibility of additional bound states contributing to the signal. We will elaborate on this possibility below.

TABLE III. Summary of branching ratios to radiative decays for $J/\psi(1S)$ and $\Upsilon(1S)$, from Ref. [34]. Decays in the last column proceed through a virtual photon.

	$\text{Br}(1^3S_1 \rightarrow (ggg, \gamma gg))$	$\text{Br}(1^3S_1 \rightarrow (\text{had}, \ell^+ \ell^-))$
$J/\psi(1S)$	(0.641, 0.088)	(0.135, 0.119)
$\Upsilon(1S)$	(0.817, 0.022)	(~ 0 , 0.075)

PHENOMENOLOGY: OTHER LHC SIGNALS

Additional bound states

So far we considered threshold production of the 1^1S_0 state η_X . As mentioned above, additional bound states of different masses may contribute to the diphoton signal. For example, in the charmonium system, $J/\psi(1S)$ decays to $\gamma + \eta_c(1S)$ with a branching ratio 0.017 ± 0.004 . The hyperfine mass splitting between the $\eta_c(1S)$ and the $J/\psi(1S)$ is approximately 113 MeV, or about 3.8% of the $\eta_c(1S)$ mass. Scaling this splitting to M yields a mass for the 1^3S_1 bound state, which we call $\Upsilon_X(1S)$ in analogy

to bottomonium, that is 30 GeV above M .⁷ Therefore, the process $\Upsilon_X(1S) \rightarrow \eta_X \gamma$, which gives a relatively soft γ , can contribute to the diphoton signal. This process also contributes to the η_X diphoton resonance. In the Low- Λ_h scenarios, the hyperfine splitting of the $1S$ state in the Coulomb approximation is given by

$$\Delta E_{\text{HF}} \equiv E_b(1^3S_1) - E_b(1^1S_0) = \frac{1}{3} C^4 \bar{\alpha}_h^4 m_X, \quad (21)$$

and can be $\mathcal{O}(10)$ GeV.

At threshold, η_X is produced through VBF while Υ_X is produced through DY.⁸ For $N_F = 0$, the possible η_X and Υ_X decay channels are

$$\begin{aligned} \eta_X &\rightarrow VV, VG_h^*, G_h G_h, \\ \Upsilon_X &\rightarrow f\bar{f}, VVV, \eta_X V, G_h V, G_h G_h^*, \end{aligned} \quad (22)$$

where V is a photon or a Z -boson, f denotes a charged SM fermion, and G_h^* is the excited 1^{+-} hidden glueball.

Among these, the process $\Upsilon_X \rightarrow l^+ l^-$ is severely constrained by LHC dilepton resonance searches [36–39], where $l = e, \mu$. These constraints imply

$$\sigma(pp \rightarrow \eta_X \rightarrow \gamma\gamma) < \frac{1.3}{K_{q\bar{q}}} \text{fb} \cdot Y_X^2 \left(\frac{C_{\gamma\gamma}}{78} \right) \frac{\text{Br}(\eta_X \rightarrow \gamma\gamma)}{\text{Br}(\Upsilon_X \rightarrow f\bar{f})}. \quad (23)$$

In the above, we have employed the bound $\sigma(pp \rightarrow \Upsilon_X \rightarrow l^+ l^-) < 1.2 \text{fb}$ at the 8 TeV LHC [36].⁹ The relevant parton luminosities are taken from Ref. [40], except for $C_{\gamma\gamma}$, which is extracted from Eq. (2), and we set $K_{\gamma\gamma} = 1$. In the Low- Λ_h region, where we can calculate the different Υ_X decay rates, we find that, for $N_F = 0$ and setting $K_{q\bar{q}} = 1$, the resulting diphoton signal is smaller than 3 fb for $\bar{\alpha}_h \gtrsim 0.2$. For larger values of N_F , higher values of $\bar{\alpha}_h$ would be allowed, since $\Gamma(\Upsilon_X \rightarrow 3g_h)$ would increase as $\alpha_h(m_X)$ increases. In the High- Λ_h case, the decay $\Upsilon_X \rightarrow G_h \gamma$ is open (see Fig. 4); however, to satisfy the constraint from Υ_X production, $\Gamma(\Upsilon_X \rightarrow G_h \gamma)$ must be enhanced by a factor of around 10 compared to the perturbative $\Gamma(\Upsilon_X \rightarrow g_h g_h \gamma)$.

Finally, radial excitations of η_X may be produced as well. If these decay directly to diphotons (rather than to η_X plus soft photons), they could lead to a broad diphoton peak, of width $\lesssim E_b$ [18]. In order to obtain the ~ 45 GeV width favored by some analyses [2], we would require intermediate values for the couplings in between the Low- Λ_h and High- Λ_h regions.

$X\text{-}\bar{X}$ pair production above threshold

Here the signatures crucially depend on the presence of light $\text{SU}(N)$ flavors. For $N_F = 0$, the models are essentially quirk models, with the quirks carrying hypercharge only. The $X\text{-}\bar{X}$ pairs will form a string of length [20]

$$r \sim \frac{E}{\Lambda^2}, \quad (24)$$

where E is the quirk-pair energy. In all our models, this string is microscopic:

$$r \ll 1 \mu\text{m}. \quad (25)$$

The quirk pair will then promptly annihilate into photons. Note that the $X\text{-}\bar{X}$ pair is produced with $L > 0$, and in principle, it could first relax to the bound state η_X , which would subsequently decay to diphotons, contributing to the diphoton resonance from η_X threshold-production. To lose angular momentum, the excited state must radiate photons or glueballs. The latter process is kinematically suppressed in the range of relatively large Λ_h we consider, so the only option is photon radiation. If this energy loss process is efficient, the signal would be relatively soft photons from the relaxation process, plus a diphoton resonance at 750 GeV. This may greatly enhance the resonance, since DY production is larger than photon fusion. However, with tight photon isolation cuts, these processes may be vetoed because of the presence of additional photons. The other possibility is that the radiation loss is not efficient, in which case X and \bar{X} annihilate without losing significant energy. This seems more plausible in our models, given the tight binding of the quirk pair by the microscopic string. The $X\text{-}\bar{X}$ pair can then go into either glueballs or photons, and the resulting photon invariant mass is simply the $X\text{-}\bar{X}$ invariant mass in this case.

Finally, the glueballs annihilate into SM particles, mainly photons, through X loops as mentioned above. These events would then have four or more photons, with di- (or tri-)photon peaks at the glueball masses.

We now consider models with additional $\text{SU}(N)$ light flavors, with mass of order Λ_h . As explained above, this is only viable in the Low- Λ_h case. The glueball lifetime is hardly affected, while the collider phenomenology as well as cosmology are different since string breaking is no longer suppressed. Consider an additional SM-singlet, $\text{SU}(N)$ fundamental field S , which can be either a scalar or a vector-like fermion. With no new couplings to SM fields, continuum $X\text{-}\bar{X}$ pair production would be followed by hadronization into $X\text{-}\bar{S}$ mesons. We refer to these mesons as ξ_S . The lightest ξ_S is charged and stable. New couplings involving X , S , and SM fields must be introduced to mediate ξ_S decays. This restricts Y_X to integer values. The possible couplings are summarized in Table IV.

⁷ This is consistent with the result expected from the confining potential, $\sim \Lambda^2/M$.

⁸ Production of more excited states (e.g., with $L > 0, n > 1$) is suppressed by their wavefunctions.

⁹ This constraint assumes $\sigma(pp \rightarrow \Upsilon_X \rightarrow l^+ l^-) \equiv \sigma(pp \rightarrow \Upsilon_X \rightarrow e^+ e^-) = \sigma(pp \rightarrow \Upsilon_X \rightarrow \mu^+ \mu^-)$.

TABLE IV. Lowest-order operators mediating ξ_S decays. ϕ_S (χ_S – $\bar{\chi}_S$) denotes a scalar (vector-like fermion) which is a SM singlet and $SU(N)$ (anti-)fundamental. SM flavor indices are omitted for simplicity. If $Y_X < 0$, replace hidden sector fields by their conjugates.

	scalar ϕ_S	vector-like fermion χ_S
$Y_X = 1$	$\phi_S(\bar{X}e^c)$	$\bar{\chi}_S X l l$
$Y_X = 2$	$\phi_S^* X u^c u^c u^c, \phi_S(\bar{X}e^c)(l l)^*$	$\chi_S \bar{X} e^c e^c$
$Y_X = 3$	$\phi_S \bar{X} e^c e^c e^c$	none up to dim-7

These decays provide various exotic signatures, with ξ_S pair production followed by ξ_S decay to 2ℓ , 3ℓ , or 3 jets, with $\ell = e, \mu$ or τ . Events with $2\ell + \cancel{E}_T$ are possible too. With the exception of the scalar coupling for $Y_X = 1$, these couplings are non-renormalizable, and therefore naturally small. Thus, bound-state formation is still important, and X particles indeed hadronize before decaying.

Still, these operators can give sufficiently high rates to evade the stringent constraints on long-lived (on detector scales) charged particles [41–43]¹⁰ if the scale by which they are suppressed is 10 TeV or higher, depending on the operator. Thus for example, for $Y_X = 2$, even the operator $(\lambda/M_{\text{high}}^3)\phi_S(\bar{X}e^c)(l l)^*$ gives

$$c\tau \sim 30 \mu\text{m} \cdot \frac{1}{\lambda^2} \left(\frac{M_{\text{high}}}{10 \text{ TeV}} \right)^6 \left(\frac{1 \text{ GeV}}{\Lambda_h} \right)^2 \left(\frac{375 \text{ GeV}}{M_{\xi_S}} \right)^5, \quad (26)$$

while the analogous operator with χ_S , allows for a higher M_{high} since it is dimension-4 only.

CONCLUSIONS

In this paper, we considered the possibility that the observed diphoton excess is due to a quarkonium-like bound state, η_X , of a hidden $SU(N)$, with fermionic constituents carrying SM hypercharge only. The production and decay of this bound state are controlled by two parameters: $Y_X^2 \alpha$, which sets the coupling strength to photons, and $C\alpha_h$, which controls the coupling to hidden gluons. These scenarios lead to a variety of multi-photon signals, and possibly exotic decays to SM fermions. Diphotons from photon-fusion production of η_X are typically accompanied by forward jets, with hadronic activity in the central region suppressed.

In large parts of the parameter space, production of the $J = 1$ Υ_X bound state leads to dilepton or dijet resonances close to 750 GeV. Without additional hidden

flavors or other dynamics, the bound Eq. (23) excludes the parameter space above $\bar{\alpha}_h \gtrsim 0.2$. For $\bar{\alpha}_h$ below 0.2, $\sigma(pp \rightarrow \Upsilon_X \rightarrow l^+ l^-)$ at the 13 TeV LHC is between 1–3 fb.

While we focused on a constituent fermion X for concreteness, our results generalize trivially to the case of a scalar X . In particular, the blue curves of Figs. 2 and 3 are barely modified, since the scalar production cross sections are down by a factor of 2 compared to the fermion case, but the signal strength scales at least as the fourth power of Y_X . On the other hand, as mentioned in the Introduction, the production of $J = 1$ bound states is suppressed in this case.

More generally, the relation between η_X and Υ_X production depends on the details of the model. For example, with N_F flavors with masses somewhat below m_X , the renormalization group running of α_h between m_X and the inverse Bohr radius is milder, resulting in larger $\alpha_h(m_X)$ for a given $\bar{\alpha}_h$. This enhances the rates of both Υ_X and η_X to hidden gluons, with the former increasing more sharply. Second, in the presence of S – X couplings to the SM, X is unstable. If the decay width Γ_X of X is comparable to roughly half the bound state width, bound state production is depleted. Since $\Gamma_{\eta_X} \gg \Gamma_{\Upsilon_X}$, the Υ_X production cross section is substantially reduced if $\Gamma_X \sim \Gamma_{\Upsilon_X}/2$, whereas η_X production is largely unaffected. Third, a hidden Z' can mediate additional Υ_X decays to hidden flavors, while its effects on η_X decays are milder.

Finally, η_X production in association with additional photons or hidden gluons is quite generic in these models, whether its source is higher resonances or continuum quirk-pair production for $N_F = 0$ models. Determining whether the diphoton resonance is accompanied by additional softer photons or missing energy is therefore crucial.

ACKNOWLEDGMENTS

We thank Yevgeny Kats, Yuri Shirman, Emmanuel Stamou, Jure Zupan, and Jonathan Rosner for useful discussions. We also thank Yevgeny Kats and David Curtin for comments on an earlier version of this manuscript. R.Z. thanks the Technion Particle Physics Center and Weizmann Institute of Science for hospitality while this work was initiated. The research of S.I., G.L., and Y.S. is supported by the Israel Science Foundation (Grant No. 720/15), by the United States–Israel Binational Science Foundation (BSF) (Grant No. 2014397), and by the ICORE Program of the Israel Planning and Budgeting Committee (Grant No. 1937/12). The work of R.Z. was partially carried out in the ILP LABEX (under reference ANR–10–LABX–63) and is supported by French state funds managed by the ANR within the Investissements d’Avenir programme under reference ANR–11–IDEX–

¹⁰ Charged particles with intermediate lifetimes, i.e., $1 \text{ mm} \lesssim c\tau \lesssim 1 \text{ m}$, are also constrained at the LHC, though less severely [44–50].

0004-02.

-
- * sho@physics.technion.ac.il
† leeg@physics.technion.ac.il
‡ yshadmi@physics.technion.ac.il
§ robert.ziegler@lpthe.jussieu.fr
- [1] ATLAS collaboration, (2015), ATLAS-CONF-2015-081.
[2] ATLAS collaboration, (2016), ATLAS-CONF-2016-018.
[3] M. Aaboud *et al.* (ATLAS), (2016), arXiv:1606.03833 [hep-ex].
[4] CMS Collaboration, (2015), CMS-PAS-EXO-15-004.
[5] CMS Collaboration, (2016), CMS-PAS-EXO-16-018.
[6] V. Khachatryan *et al.* (CMS), (2016), arXiv:1606.04093 [hep-ex].
[7] S. Fichtel, G. von Gersdorff, and C. Royon, Phys. Rev. **D93**, 075031 (2016), arXiv:1512.05751 [hep-ph].
[8] C. Csáki, J. Hubisz, and J. Terning, Phys. Rev. **D93**, 035002 (2016), arXiv:1512.05776 [hep-ph].
[9] C. Csáki, J. Hubisz, S. Lombardo, and J. Terning, Phys. Rev. **D93**, 095020 (2016), arXiv:1601.00638 [hep-ph].
[10] K. Harigaya and Y. Nomura, Phys. Lett. **B754**, 151 (2016), arXiv:1512.04850 [hep-ph].
[11] Y. Nakai, R. Sato, and K. Tobioka, Phys. Rev. Lett. **116**, 151802 (2016), arXiv:1512.04924 [hep-ph].
[12] D. Curtin and C. B. Verhaaren, Phys. Rev. **D93**, 055011 (2016), arXiv:1512.05753 [hep-ph].
[13] P. Agrawal, J. Fan, B. Heidenreich, M. Reece, and M. Strassler, (2015), arXiv:1512.05775 [hep-ph].
[14] C. Han, K. Ichikawa, S. Matsumoto, M. M. Nojiri, and M. Takeuchi, JHEP **04**, 159 (2016), arXiv:1602.08100 [hep-ph].
[15] K. Harigaya and Y. Nomura, JHEP **03**, 091 (2016), arXiv:1602.01092 [hep-ph].
[16] Y. Kats and M. J. Strassler, JHEP **05**, 092 (2016), arXiv:1602.08819 [hep-ph].
[17] K. Harigaya and Y. Nomura, (2016), arXiv:1603.05774 [hep-ph].
[18] J. F. Kamenik and M. Redi, (2016), arXiv:1603.07719 [hep-ph].
[19] P. Ko, C. Yu, and T.-C. Yuan, (2016), arXiv:1603.08802 [hep-ph].
[20] J. Kang and M. A. Luty, JHEP **11**, 065 (2009), arXiv:0805.4642 [hep-ph].
[21] K. Cheung, W.-Y. Keung, and T.-C. Yuan, Nucl. Phys. **B811**, 274 (2009), arXiv:0810.1524 [hep-ph].
[22] N. Craig, P. Draper, C. Kilic, and S. Thomas, (2015), arXiv:1512.07733 [hep-ph].
[23] J. F. Kamenik, B. R. Safdi, Y. Soreq, and J. Zupan, (2016), arXiv:1603.06566 [hep-ph].
[24] Y. Kats and M. J. Strassler, JHEP **11**, 097 (2012), arXiv:1204.1119 [hep-ph].
[25] C. J. Morningstar and M. J. Peardon, Phys. Rev. **D60**, 034509 (1999), arXiv:hep-lat/9901004 [hep-lat].
[26] Y. Chen *et al.*, Phys. Rev. **D73**, 014516 (2006), arXiv:hep-lat/0510074 [hep-lat].
[27] J. E. Juknevich, D. Melnikov, and M. J. Strassler, JHEP **07**, 055 (2009), arXiv:0903.0883 [hep-ph].
[28] J. E. Juknevich, JHEP **08**, 121 (2010), arXiv:0911.5616 [hep-ph].
[29] E. Eichten, S. Godfrey, H. Mahlke, and J. L. Rosner, Rev. Mod. Phys. **80**, 1161 (2008), arXiv:hep-ph/0701208 [hep-ph].
[30] K. Hagiwara, K. Kato, A. D. Martin, and C. K. Ng, Nucl. Phys. **B344**, 1 (1990).
[31] S. Kim, Phys. Rev. **D92**, 094505 (2015), arXiv:1508.07080 [hep-lat].
[32] N. D. Barrie, A. Kobakhidze, S. Liang, M. Talia, and L. Wu, (2016), arXiv:1604.02803 [hep-ph].
[33] A. A. Penin and M. Steinauser, Phys. Lett. **B538**, 335 (2002), arXiv:hep-ph/0204290 [hep-ph].
[34] K. A. Olive *et al.* (Particle Data Group), Chin. Phys. **C38**, 090001 (2014).
[35] S. Aoki *et al.*, Eur. Phys. J. **C74**, 2890 (2014), arXiv:1310.8555 [hep-lat].
[36] G. Aad *et al.* (ATLAS), Phys. Rev. **D90**, 052005 (2014), arXiv:1405.4123 [hep-ex].
[37] V. Khachatryan *et al.* (CMS), JHEP **04**, 025 (2015), arXiv:1412.6302 [hep-ex].
[38] CMS Collaboration, (2015), CMS-PAS-EXO-15-005.
[39] ATLAS collaboration, (2015), ATLAS-CONF-2015-070.
[40] R. Franceschini, G. F. Giudice, J. F. Kamenik, M. McCullough, A. Pomarol, R. Rattazzi, M. Redi, F. Riva, A. Strumia, and R. Torre, JHEP **03**, 144 (2016), arXiv:1512.04933 [hep-ph].
[41] S. Chatrchyan *et al.* (CMS), JHEP **07**, 122 (2013), arXiv:1305.0491 [hep-ex].
[42] G. Aad *et al.* (ATLAS), JHEP **01**, 068 (2015), arXiv:1411.6795 [hep-ex].
[43] CMS Collaboration, (2015), CMS-PAS-EXO-15-010.
[44] G. Aad *et al.* (ATLAS), Phys. Rev. **D88**, 112006 (2013), arXiv:1310.3675 [hep-ex].
[45] G. Aad *et al.* (ATLAS), Phys. Rev. **D90**, 112005 (2014), arXiv:1409.5542 [hep-ex].
[46] V. Khachatryan *et al.* (CMS), Phys. Rev. **D91**, 052012 (2015), arXiv:1411.6977 [hep-ex].
[47] V. Khachatryan *et al.* (CMS), JHEP **01**, 096 (2015), arXiv:1411.6006 [hep-ex].
[48] G. Aad *et al.* (ATLAS), Phys. Rev. **D92**, 072004 (2015), arXiv:1504.05162 [hep-ex].
[49] G. Aad *et al.* (ATLAS), Eur. Phys. J. **C75**, 407 (2015), arXiv:1506.05332 [hep-ex].
[50] M. Aaboud *et al.* (ATLAS), (2016), arXiv:1604.04520 [hep-ex].